PHYSICAL REVIEW A VOLUME 22, NUMBER 4 OCTOBER 1980

Muonic cascade: General discussion and application to the third-row elements

P. Vogel
Physics Department, California Institute of Technology, Pasadena, California 91125
(Received 19 February 1980)

The experimental data on muonic x-ray intensities for the third-row atoms ($Z = 11$–17) are analyzed in a unified way. The deduced initial l distributions are not very far from the statistical ones; they are, however, somewhat steeper near the closed atomic shells and somewhat flatter in the middle of the shell. The K-electron refilling rate is fast increasing with Z; it is considerably smaller than the refilling rate of normal neutral atoms. The calculation shows that in these light atoms the inner electron shells (K and L) are strongly perturbed during the muonic cascade. Correct treatment of their depletion and refilling is essential. The two existing computer cascade programs are compared. It is stressed that a correct treatment of penetration effects as well as inclusion of quadrupoles in the Auger electron emission is necessary when one wants to utilize the full accuracy of the experimental data.

I. INTRODUCTION

The muonic, pionic, kaonic, and other exotic atoms are by now familiar tools widely used in studies of nuclear sizes and shapes, meson-nuclear interactions, QED tests, etc. The x-ray transition energies are well understood and can be calculated with great accuracy. However, the initial formation of such an atom, in which the meson is captured from the continuum into a bound state, is not yet fully understood. Similarly, one does not have a complete theory of the subsequent cascade. On the other hand, the amount of reliable data on muon capture and cascade is rapidly increasing. Among the various problems in this complex process, perhaps the most amenable one to analysis is the "quantum cascade," that is, the muon transitions between states with relatively small quantum numbers. The starting point of the quantum cascade is the point where the classical description breaks down and the transition energy becomes a large fraction of the binding energy. Alternatively, and to a large extent equivalently, the quantum cascade begins when radiation of an observable intensity is first emitted at $n = 15$–20. The theoretical analysis of the cascade is relatively simple because the muon wave functions are to a good approximation hydrogenlike, while the electron wave functions are those of the $Z - 1$ atom.

The cascade proceeds by the emission of the Auger electrons from the electron K, L, and M shells and by the muonic x-ray emission. The main transition strength is in only one of these possible modes at any given time. Radiation is dominant at low quantum numbers ($n \lesssim 5$ for the considered atoms). At higher quantum numbers the Auger transitions dominate, with the main strength being in the $\Delta n = 1$ Auger emission from the electron shells with binding energy closest to the $\Delta n = 1$ transition energy. Thus, for the $Z = 11$–17 atoms considered here, the L-electron emission dominates for $n \geq 10$, and the K-electron emission dominates for $9 \geq n \geq 5$.

The partial radiative and Auger transition probabilities were first calculated by Burbidge and de Borde[1] and by Eisenberg and Kessler.[2] They were incorporated into the so-called Hüfner cascade code.[3] Recently, a new version of this program was written by Akylas and Vogel,[4] including higher multipoles (quadrupole and octupole), higher shells (M shell), as well as treatment of the penetration part of the Auger matrix elements.

In our numerical calculations reported below we begin the cascade at $n = 17$. According to our results the muon emits during the cascade 4–5 L electrons, ~5 K electrons, and ~2 muonic x rays, that is, it makes altogether about 11 quantum jumps. Because normal atoms have 8 L electrons and 2 K electrons these shells are strongly perturbed during the cascade and their refilling must be considered. In particular, the K refilling is of crucial importance.

The observable quantities in a muon cascade are the x rays. In a typical experiment the intensities of 5–10 of the lowest members in each of the Lyman, Balmer, and sometimes higher series are measured. The purpose of the analysis is to relate these observables to the relevant physical parameters, that is to the population of the various muonic states in the beginning of the cascade and to parameters describing the electron refilling. It is customary, and supported by experimental evidence,[5] to assume that there is very little direct capture into states with $n \leq 20$. The initial muon population should be, therefore, normalized to unity. The shape of the muon l distribution varies slowly between states with sufficiently large n. Consequently, one may assume that the entire muon initial population is concentrated

TABLE I. Intensities of muonic x rays in Na per 100 stopped muons. Calculated for $n_{init}=17$, $P(l)=(0.455+0.268l+0.037l^2)\times10^{-2}$, $\Gamma_K=0.06$ eV.

	$n\rightarrow1$		$n\rightarrow2$		$n\rightarrow3$		$n\rightarrow4$
n	Expt.[a]	Calc.	Expt.	Calc.	Expt.	Calc.	Calc.
2	79.2(1.0)	79.27					
3	8.52(17)	8.52		60.6			
4	5.74(14)	5.88		11.27		33.2	
5	3.74(11)	3.60		3.74		4.17	8.96
6	1.61(8)	1.65		1.19		1.01	1.15
7	0.66(6)	0.65		0.40		0.31	0.30
8	0.17(6)	0.22		0.13		0.09	0.08
9		0.04		0.02		0.02	0.01
10		0.08		0.04		0.03	0.02
>10		0.08		0.04		0.03	0.02

[a] Experimental data from Ref. 11 for Na metal. Normalized to 100% of Lyman series. Resulting $\chi^2/DF=\frac{3.5}{4}$.

in states with a single n value. We shall examine this assumption in Sec. III. The "initial l distribution" must be a smooth function of l and may be parametrized by one or two parameters. Adding one parameter each describing the population or refilling of the electronic K and L shells, one ends up with 3–4 physical parameters describing the cascade.

Experimental data are available now for a more or less complete analysis of the elements in the third row of the periodic table ($Z=11-17$). We would like to know whether a consistent approach is possible, and whether the resulting parameters vary smoothly with Z. We would like to compare the resulting l distribution with the statistical l distribution predicted by the classical approach to muon capture.[6,7] There is evidence[8-10] that the initial l distribution exhibits periodic variations; that is, the average initial angular momentum is larger for atoms with nearly closed valence electron shells than for atoms with half filled valence shells. We would like to see whether our detailed analysis supports this evidence.

The numerical calculations are described and discussed in Sec. II. In Sec. III we analyze in more detail the various effects included in our treatment of the cascade but neglected in most previous analyses.

II. CASCADE CALCULATION

For our numerical analysis we chose the data of Refs. 5 and 11–14 on the third-row elements, Na, Mg, Al, P, S, and Cl. (For detailed infor-

TABLE II. Intensities of muonic x rays in Mg per 100 stopped muons. Calculated for $n_{init}=17$, $P(l)=(1.12+0.76l+0.047l^2)\times10^{-2}$, $\Gamma_K=0.10$ eV.

	$n\rightarrow1$		$n\rightarrow2$		$n\rightarrow3$		$n\rightarrow4$
n	Expt.[a]	Calc.	Expt.[a]	Calc.	Expt.[a]	Calc.	Calc.
2	79.58(65)	79.61					
3	7.79(27)	7.86	62.5(2.7)	60.30			
4	5.30(25)	5.39	10.4(1.3)[b]	11.28	36.0(5.6)[b]	35.77	
5	3.73(19)	3.73	4.26(36)	4.12	4.90(40)[b]	4.66	9.93
6	2.12(14)	1.94	1.16(30)[b]	1.40	1.81(30)[b]	1.16	1.26
7	0.86(5)	0.82	0.30(7)	0.49	0.47(12)	0.36	0.32
8	0.29(3)	0.31	0.17(6)[b]	0.10	0.10(6)[b]	0.11	0.09
9	0.09(3)	0.06	0.43(16)	0.03		0.02	0.02
10	0.09(3)	0.13		0.07	0.07(4)	0.04	0.03
11	0.055(16)	0.053	0.26(7)[b]	0.03		0.02	0.01
12	0.038(13)	0.022		0.01		0.02	0.005
13	0.021(12)	0.011		0.01		0.003	0.002
14	0.016(12)	0.012	0.19(8)	0.006		0.004	0.003
>14	0.028(18)	0.04		0.020		0.012	0.010

[a] Experimental data from Ref. 5. Resulting $\chi^2/DF=\frac{39}{26}$.
[b] Lines affected by interference with C, O, and N. When excluded $\chi^2/DF=\frac{22}{18}$.

TABLE III. Intensities of muonic x rays in Al per 100 stopped muons. Calculated for $n_{init}=17$, $P(l)=(1.40+0.096l+0.042l^2)\times10^{-2}$, $\Gamma_K=0.10$ eV.

	$n\to1$		$n\to2$		$n\to3$		$n\to4$
n	Expt.[a]	Calc.	Expt.[a]	Calc.	Expt.[a]	Calc.	Calc.
2	79.65(60)	79.74					
3	7.43(29)	7.37	62.5(1.8)	59.86			
4	4.72(20)	4.76	9.7(1.9)	11.09	33.5(5.3)	39.08	
5	3.89(17)	3.74	4.23(32)	4.61	6.07(70)	5.59	12.4
6	2.35(11)	2.30	1.44(19)	1.79	1.98(51)	1.52	1.67
7	1.13(8)	1.12	0.65(7)	0.68	0.55(3)	0.50	0.45
8	0.37(8)	0.45	0.21(6)	0.24	0.12(4)	0.16	0.13
9	0.18(8)	0.10	0.21(15)	0.05	0.02(2)	0.03	0.02
10	0.12(8)	0.20		0.10		0.06	0.05
11	0.08(8)	0.08	0.07(6)	0.04		0.02	0.02
12		0.04		0.02		0.01	
13		0.02		0.05	0.05(5)	0.03	
14	0.08(8)	0.02	0.10(10)				0.03
>14		0.07					

[a] Experimental data from Ref. 5. Resulting $\chi^2/DF=\frac{23}{24}$.

mation see captions of Tables I–VI.) Whenever possible we used the data on pure elements. The x-ray intensities often depend on the chemical or crystalline form of the target. The differences in x-ray intensities between various forms of the same element are, however, typically only 1–2 standard deviations and were not considered here.

The following standard procedure has been adopted.

(a) The cascade calculation began at $n=17$ where the electron L shell is open for Auger $\Delta n=1$ transition for all considered atoms. The effect of electron M shell is always small and was not included in the calculation.

(b) The initial l distribution was characterized by the two-parameter formula

$$P(l)=\frac{1}{n}+b[l-\tfrac{1}{2}(n-1)]+c[l^2-\tfrac{1}{6}(n-1)(2n-1)], \quad (1)$$

where b and c are adjustable parameters and n is the initial main quantum number. More physically meaningful parameters are the first and second moments of $P(l)$, namely,

TABLE IV. Intensities of muonic x rays in P per 100 stopped muons. Calculated for $n_{init}=17$, $P(l)=(1.035+0.54l+0.006l^2)\times10^{-2}$, $\Gamma_K=0.17$ eV.

	$n\to1$		$n\to2$		$n\to3$		$n\to4$
n	Expt.[a]	Calc.	Expt.[a]	Calc.	Expt.	Calc.	Calc.
2	75.2(1.9)	79.16					
3	7.25(19)	7.29	54.5(3.3)	57.56			
4	4.04(11)	4.15	10.81(31)	10.99		40.96	
5	3.85(11)	3.73	4.67(23)	5.48		7.07	15.23
6	2.74(8)	2.71	2.62(10)	2.53		2.20	2.36
7	1.49(5)	1.46	1.20(6)	1.03		0.76	0.67
8	0.44(5)	0.63	0.30(5)	0.38		0.26	0.21
9		0.14		0.08		0.05	0.04
10		0.32		0.18		0.12	0.09
11		0.14		0.07		0.05	0.03
12		0.06		0.03		0.02	0.01
13		0.03		0.02		0.01	0.01
14		0.04		0.02		0.01	0.01
>14		0.12		0.06		0.04	0.03

[a] Experimental data of Ref. 12 for red phosphorus. Errors for transitions originating in $n=7$ and 8 adjusted. Resulting $\chi^2/DF=\frac{47}{10}$.

TABLE V. Intensities of muonic x rays in S per 100 stopped muons. Calculated for $n_{\text{init}} = 17$, $P(l) = (1.53 + 0.257l + 0.026l^2) \times 10^{-2}$, $\Gamma_K = 0.22$ eV.

	$n \to 1$		$n \to 2$		$n \to 3$		$n \to 4$
n	Expt.[a]	Calc.	Expt.	Calc.	Expt.	Calc.	Calc.
2	80.7(1.0)	80.74					
3	6.86(20)	6.78		60.01			
4	3.31(16)	3.46		10.31		44.20	
5	3.31(16)	3.20		5.14		7.38	17.68
6	2.58(16)	2.54		2.53		2.32	2.60
7	1.45(12)	1.51		1.09		0.82	0.73
8	0.62(6)	0.70		0.43		0.29	0.23
9	0.33(6)	0.17		0.10		0.06	0.05
10	0.30(7)	0.38		0.22		0.14	0.10
11		0.17		0.09		0.06	0.04
12		0.08		0.04		0.02	0.02
13	0.50(7)	0.04		0.02		0.01	0.01
14		0.05		0.02		0.02	0.01
>14		0.16		0.08		0.05	0.03

[a] Experimental data from Ref. 13 for Na_2S. Normalized for 100% of Lyman series. Resulting $\chi^2/DF = \frac{12}{7}$.

$$\bar{l} \equiv \sum P(l) l = \tfrac{1}{2}(n-1) + \tfrac{1}{6}(n-1)n(n+1)[b + (n-1)c], \tag{2}$$

$$\bar{l}^2 \equiv \sum P(l) l^2 = \tfrac{1}{6}(n-1)(2n-1) + \tfrac{1}{12}(n-1)n[(n^2-1)b + \tfrac{1}{15}(2n-1)(8n^2-3n-11)c]. \tag{3}$$

Note that for the statistical distribution one has $c = 0$ and $b = 2/n^2$. We have determined the best-fit values of b and c, respectively, $\bar{l}$ and $\bar{l}^2$ (see Fig. 1). The two-parameter formula (1) gives better χ^2/DF than the often used single-parameter modified statistical distribution.

(c) The refilling of the electron K shell was characterized by the K-electron refilling width Γ_K. The formalism of treatment of the K-electron refilling has been described in Ref. 15. The neglect of possible variation in Γ_K during the cascade is justified, because the K-electron emission is dominant only during a relatively short and well-defined stage of the cascade. The width Γ_K is

TABLE VI. Intensities of muonic x rays in Cl per 100 stopped muons. Calculated for $n_{\text{init}} = 17$, $P(l) = (0.702 + 0.085l + 0.015l^2) \times 10^{-2}$, $\Gamma_K = 0.4$ eV.

	$n \to 1$		$n \to 2$		$n \to 3$		$n \to 4$
n	Expt.[a]	Calc.	Expt.[a]	Calc.	Expt.	Calc.	Calc.
2	85.8(1.0)	85.20					
3	6.27(26)	6.13	67.6(1.7)	66.43			
4	2.66(17)	2.67	10.1(1.5)	10.05		50.38	
5	2.40(17)	2.26	5.13(74)	4.57		7.66	20.76
6	1.97(17)	1.70	1.76(27)	2.08		2.17	2.67
7	0.86(17)	0.95	0.61(14)	0.82		0.68	0.66
8		0.42		0.30		0.22	0.20
9		0.11		0.07		0.05	0.04
10		0.22		0.14		0.10	0.08
11		0.11		0.07		0.05	0.04
12		0.03		0.02		0.01	0.01
13		0.04		0.02		0.01	0.01
14		0.04		0.02		0.01	0.01
>14		0.12		0.06		0.04	0.03

[a] Experimental data from Ref. 14 for $CaCl_2$. Normalized to 100% of Lyman series and using $L\alpha = K\alpha / \sum_{l>\alpha}(1 + L_l/L\alpha)$. Resulting $\chi^2/DF = \frac{8.9}{8}$.

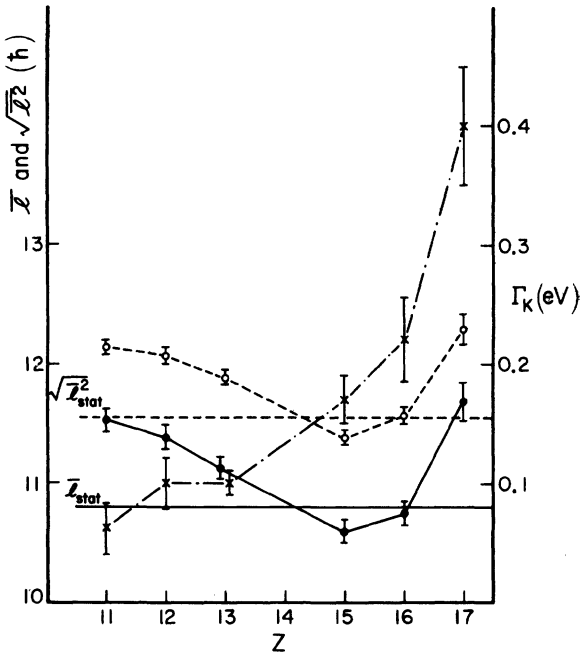

FIG. 1. Cascade characteristics of various atoms. The quantity $\bar{l}$ is denoted by closed circles connected by the solid line; $(\bar{l}^2)^{1/2}$ is denoted by open circles connected by the dashed line. The left scale is used for these quantities. Γ_K is denoted by crosses and connected by dot-dashed line; the right scale is used. The $\bar{l}$ and $(\bar{l}^2)^{1/2}$ for statistical distribution are also shown for comparison.

restricted to the interval between zero for a fully ionized atom in a vacuum and its value of a neutral atom. This $\Gamma_K^{neutral}$ could be deduced from the calculated radiative emission rates and from fluorescence yields ω_K,

$$\Gamma_K^{neutral} = \Gamma_{rad}/\omega_K . \quad (4)$$

For the considered atoms $\Gamma_K^{neutral}$ raises gradually from 0.25 eV for Na to 0.60 eV for Cl. The resulting best-fit Γ_K values, shown in Fig. 1, are smaller than $\Gamma_K^{neutral}$, suggesting depletion of the electron L shell. Nevertheless, the best fit Γ_K values correspond to the refilling rate which is fast enough that about five Auger K-electron transitions are possible during the cascade.

(d) To describe the L-electron depletion and refilling we chose a single parameter for *all* considered atoms, the effective number of L electrons, pop$(L)=0.3$. This means that all L-electron emission rates were multiplied by a single reduction factor 0.3. Otherwise the number of L electrons was left constant during the cascade. The x-ray intensities do not depend very sensitively on this number which is determined to about 30% accuracy. The value 0.3 is near the minimum of χ^2 in all cases.

Our choice of parametrization of the L-shell effects is partially based on practical considerations, that is, reduction of the number of free parameters and convenience of the lengthy computer calculations. Formally it is not completely satisfactory, but a better treatment is impossible until the electron $2s$ and $2p$ shells are considered separately. The $2s$ and $2p$ electrons are lumped together in the cascade programs.[3,4] However, the $2s$ electrons are fast refilled in neutral atoms and dominate the cascade for $13 < n < 10$. On the other hand, the $2p$ electrons are slowly refilled in neutral atoms and are depleted in two stages, first early in the cascade for $n > 13$ and then as a source of K-electron depletion for $n < 10$. Our choice of parametrization is a compromise reflecting most simply the overall effect.

In the numerical calculation we used an automated version of our computer code.[4] Multipoles up to quadrupole were included as well as the penetration effect (see discussion in Sec. III).

The best-fit initial l distribution and Γ_K values are shown in Tables I–VI together with the calculated and experimental x-ray intensities of the first four x-ray series. Good overall fit is obtained in Na, Al, and Cl, and somewhat worse fit is obtained in Mg and S. The resulting χ^2/DF is too large in P. The error bars of transitions originating in $n=7$ and 8 of P were adjusted so that these transitions do not completely dominate the resulting χ^2. Let us stress, however, that in all cases the fitted b, c, and Γ_K values are well defined and χ^2 has a minimum.

The Mg and Al cascade was analyzed earlier in Ref. 5 using the older version of the cascade program. Despite this difference and other smaller variations in approach the overall conclusions of both analyses agree quite well.

The Z dependence of the resulting parameters is summarized in Fig. 1. The Γ_K value is increasing with Z faster than the $\Gamma_K^{neutral}$; the corresponding reduction decreases from 4 in Na to 1.5 in Cl. Such a tendency is reasonable and reflects the increasing number of electrons available for refilling.

The initial l distributions are the most interesting lessons of the present analyses. It is important to note that their first and second moments differ by only ~10% from the corresponding values for the statistical l distribution (Fig. 1). These relatively small deviations are certainly within limits of the classical approach. On the other hand one has to remember that the fitting procedure is directly sensitive to only small l values, because only the Lyman and Balmer series are usually experimentally known. The full

initial l distribution thus depends on our (sensible) assumption of smoothness and on our parametrization [Eq. (1)].

The second interesting feature of these l distributions is their u-shaped Z dependence. The l distribution near closed shells, in Na and Cl, is steeper than the statistical one, while in the middle, for phosphorus, it is flatter. Our more complete analysis thus confirms the trend noted earlier in Refs. 8–10 and elsewhere. There is no theoretical explanation of this effect available at the present time. It would be interesting to see whether muonic Si follows the overall trend shown in Fig. 1.

The population of the electron K shell during the various stages of the cascade is illustrated in Fig. 2. The dip at $n=5$–8, where transitions proceed mostly by the K-electron emission, is clearly visible.

The K-electron vacancies affect not only the x-ray intensities but, via electron screening, the x-ray energies as well. The electron screening of the $4f$-$3d$ transition in muonic Si has recently been determined[16] as having only 0.47 ± 0.11 of its calculated neutral atom value. Our calculation (average of P and Al) predicts K population ~0.58 in agreement with the experiment. Note that Fig. 2 shows the number of K electrons present when muon reaches the n,l state, while the mentioned experiment measures a somewhat larger number of K electrons present during the subsequent transition.

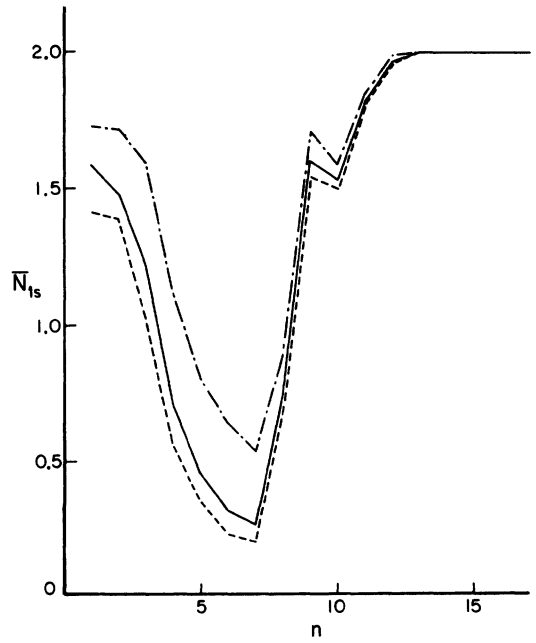

FIG. 2. Population of the electronic $1s$ state when muon reaches the spherical $n,l=n-1$ state. Notation: dashed line—Na; solid line—Al; dot-dashed line—Cl.

To visualize the development of the cascade we show in Fig. 3 the population of various selected states in muonic aluminum. The curve P_{tot} describes the total population of all states with the same principal quantum number n. As noted earlier the cascade consists of about 11 quantal jumps, giving $\Delta n\sim1.5$ per step. The average P_{tot} is therefore ~0.75.

In this context one may ask how much our assumption $P_{tot}(n_{init})=1$ affects the resulting cascade. Our program allows distribution of the initial population over several n values. We have verified that the x-ray intensities vary by less than 2% when the muons are evenly distributed among $n=17$, 16 or $n=17$, 16, 15 instead of being restricted to $n=17$. The l-distribution shapes were identical in all these cases. Thus, for the considered atoms the restriction of the initial population to a single n value is justified.

The other curves in Fig. 3 show the population of the spherical orbits ($l=n-1$, P_{sph}) and of the strongly eccentric p orbits (P_{np}). The increase of P_{sph} is caused not only by the decreasing number of available l states but also by the increasing steepness of the l distribution with decreasing n. The P_{np} population determines the intensity of the Lyman x-ray series

$$I(np-1s)=P_{np}\Gamma_R/\Gamma\,. \tag{5}$$

The branching ratio Γ_R/Γ increases from 0.02 at $n=17$ to 0.1 at $n=11$, and saturates to ~1.0 at $n=6$.

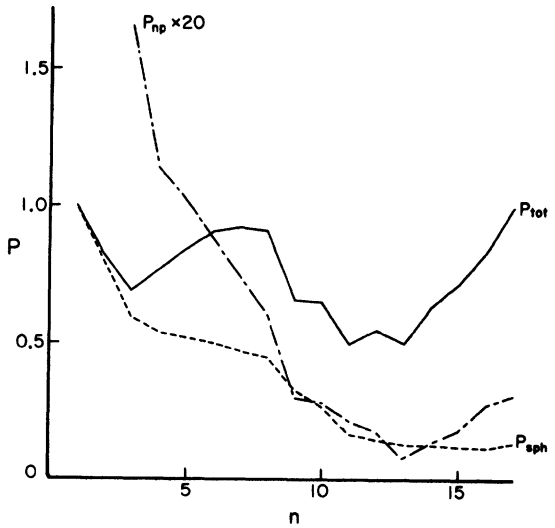

FIG. 3. Cascade characteristics in Al. P_{tot} is the total population of all states with a given n value; P_{sph} is the population of the spherical state $l=n-1$; P_{np} is the population of the np state (the quantity shown is $20\times P_{np}$).

III. FORMALISM OF THE CASCADE ANALYSIS: ROLE OF VARIOUS TERMS

In this section we summarize previously unpublished formulas and discuss the relative importance of various terms contributing to the total transition rate. Many of the original results were first obtained by Akylas[17] and are incorporated in the cascade program.[4]

Throughout we use the hydrogenlike nonrelativistic wave functions for the bound muon, as well as for the bound and continuum electrons. To simulate the screening effect of other electrons we use an effective charge Z_K^* (Z_L^*, Z_M^*) in the electronic wave functions of the $K(L,M)$ electrons and of the corresponding continuum states. The Z^* values were chosen in our numerical calculations in a following way: First we calculated an analog of the electric-dipole internal conversion coefficient (ICC) using our approximate electron wave functions. The Z^* is then chosen in such a way that these ICC agree with the precise values[18] over the energy range of interest. The choice

$$Z_K^* = 0.975Z, \quad Z_L^* = 0.95Z - 2.5$$

fulfills these requirements very well for $10 \leq Z \leq 30$. This procedure, which we propose as a standard in future muonic cascade analyses, assures that the most important Auger rate is treated correctly.

Several smaller effects are not included in the cascade program,[4] and consequently in the present treatment. They include the dynamic electron screening, described by Leon and Seki,[19] relativistic, and nuclear finite-size corrections. All of them could influence the radiative and Auger transition rates to some extent. If the experimental accuracy is further improved, it would be necessary to treat also these, computationally very complicated effects.

The muonic radiative $n_1 l_1 \to n_2 l_2$ transition probability for multipolarity L is equal to

$$\Gamma_R^L = \frac{2(L+1)(2L+1)(2l_2+1)}{L[(2L+1)!!]^2} \begin{pmatrix} l_1 & L & l_2 \\ 0 & 0 & 0 \end{pmatrix}^2 \times \alpha c \left(\frac{\omega}{c}\right)^{2L+1} I_L^2 . \tag{6}$$

Here α is the fine-structure constant, c is the velocity of light, $\omega = \Delta E/\hbar$ is the transition frequency, and the radial integral I_L is equal to

$$I_L = \tfrac{1}{2}\left(\frac{a_\mu}{2Z}\right)^L \sum_{M_1=l_1}^{n_1-1} \sum_{M_2=l_2}^{n_2-1} \frac{(-1)^{M_1+M_2-l_1-l_2}}{n_1^{M_1+2} n_2^{M_2+2}} \left(\frac{2n_1 n_2}{n_1+n_2}\right)^{M_1+M_2+L+3} \times \frac{[(n_1+l_1)!(n_1-l_1-1)!(n_2+l_2)!(n_2-l_2-1)!]^{1/2}}{(n_1-M_1-1)!(l_1+M_1+1)!(M_1-l_1)!(n_2-M_2-1)!(l_2+M_2+1)!(M_2-l_2)!} . \tag{7}$$

In Eq. (7) a_μ is the muonic Bohr radius

$$a_\mu = (m_e/m_\mu)a_0 = 255.93 , \tag{8}$$

expressed in fm. In practice, only the dipole radiation is usually important, the quadrupole one being suppressed by a factor $\sim(Z\alpha/n)^2$.

The Auger transition involves the same change in muon quantum numbers plus an ejection of bound electron from the n', l' state into the continuum state with wave number k and angular momentum l. The corresponding probability per electron is given by

$$\Gamma_A^L = \frac{(2l_2+1)(2l+1)}{2L+1} \begin{pmatrix} l_1 & L & l_2 \\ 0 & 0 & 0 \end{pmatrix}^2 \begin{pmatrix} l' & L & l \\ 0 & 0 & 0 \end{pmatrix}^2 [I_L I_{el} - I_{pen}]^2 . \tag{9}$$

The same muonic radial integral I_L [Eq. (7)] enters here. The second term in square brackets above involves coupled integrals and represents the "penetration" of the electron through the muon orbit. The electronic radial integral I_{el} in the first term is given by

$$I_{el} = \left(\frac{\alpha c}{a_0}\right)^{1/2} \left(\frac{Z^*}{a_0}\right)^L \left(\frac{2}{y}\right)^{l+1} e^{(1/2)\pi y} \frac{|\Gamma(l+1-iy)|}{(2l+1)!} \left(\frac{(n'+l')!(n'-l'-1)!y}{2n'}\right)^{1/2} \times \sum_{M'=l'}^{n'-1} \left(\frac{2}{n'}\right)^{M'+3/2} \frac{(-1)^{M'-l'}(M'+l+1-L)! F[l+1+iy;\ M'+l+2-L;\ 2l+2;\ 2in'/(y+in')]}{(n'-M'-1)!(l'+M'+1)!(M'-l')!(1/n'+i/y)^{M'+l+2-L}} . \tag{10}$$

We use here the dimensionless quantity

$$y = Z^*/ka_0 \tag{11}$$

instead of the wave number k. The expression (10) is real and the expansion of the hypergeometric function contains only a finite number of terms for $n' \leq 3$, $L \leq 3$. Furthermore, Γ_A always reaches its maximum at threshold ($y \to \infty$). In order to treat the second term in Eq. (9) we have to evaluate the coupled

radial integral

$$I_{\rm pen}=\int_0^\infty R^*_{n_2 l_2}(r_\mu)R_{n_1 l_1}(r_\mu)r_\mu^2\,dr_\mu\int_0^{r_\mu}R^*_{k,l}(r_e)R_{n'l'}(r_e)\left(\frac{r_\mu^L}{r_e^{L+1}}-\frac{r_e^L}{r_\mu^{L+1}}\right)r_e^2\,dr\,. \tag{12}$$

Although analytical evaluation of $I_{\rm pen}$ is possible, it is impractical because it involves summations of long fast-oscillating series. On the other hand, one needs to evaluate $I_{\rm pen}$ only for reasonably large y values, that is, near the threshold. It turns out that one could expand in powers of the parameter

$$v=\frac{Z^*m_e}{Zym_\mu\left(\frac{1}{n_1}+\frac{1}{n_2}\right)}\ll 1\,, \tag{13}$$

and that the corresponding series converges rapidly. In Refs. 4 and 17 the incomplete integral in Eq. (12) is rewritten as

$$g(r_\mu)=\left(\frac{\alpha c}{a_0}\right)^{1/2}\frac{(2l+1)!\,|\Gamma(l+1-iy)|}{(2y)^{l+1/2}}\left(\frac{(n'+l')!\,(n'-l'-1)!}{n'}\right)^{1/2}e^{(1/2)\pi y}$$
$$\times\sum_{M'=l'}^{n'-1}\sum_{j=0}^{\infty}\left(\frac{2}{n'}\right)^{M'+3/2}\frac{(-1)^{M'-l'}}{(n'-M'-1)!\,(l'+M'+1)!\,(M'-l')!}A_j$$
$$\times\int_0^{rZ^*/a_0}\rho^{M'+2+(j-1)/2}\exp(-\rho/n')\left(\frac{\rho_\mu^L}{\rho^{L+1}}-\frac{\rho^L}{\rho_\mu^{L+1}}\right)J_{2l+1+j}(2\sqrt{2\rho})\,d\rho\,. \tag{14}$$

Here $J_n(t)$ are the Bessel functions and $\rho_\mu=r_\mu Z^*/a_0$. The first four expansion coefficients are

$$A_0=1,\quad A_1=0,\quad A_2=-\frac{(l+1)}{2y^2},\quad A_3=\frac{1}{3\sqrt{2}\,y^2}\,. \tag{15}$$

In our cascade program[4] each of the integrals in Eq. (14) is approximated by a simple function

$$I(\tau)=\beta\tau^{M'+l+2+j}\exp(-\alpha\tau a_0/a_\mu)\,, \tag{16}$$

where α and β are fitted parameters, independent of Z, Z^*, and of muon mass. They are chosen in such a way that the integral in Eq. (14) is close (within 1%) to its exact value in the important region $0\le r\le a_0/Z$. In practice, already the $j=0$ term accounts for ~95% of the full value. The remaining integration over r_μ in Eq. (12) is straightforward, leading to formulas analogous to and only slightly more complicated than the integral I_L in Eq. (7). The fitted parameters are close to their simple estimates, namely, $\alpha\simeq m_e/m_\mu$ and

$$\beta\simeq\frac{2^{l+(j+1)/2}(2L+1)}{(2l+1+j)!\,(M'+l+2+j-L)(M'+l+3+j+L)}\,. \tag{17}$$

A different approach, roughly equivalent to the assumption $j=0$ in Eq. (14) was used by Bingeli[20] in his treatment of the monopole transitions.

The "Hüfner cascade"[3] also includes penetration in the $L=0$ monopole case (where the leading term vanishes, $I_{L=0}=0$). However, that program not only uses $\alpha=0$ in Eq. (16) but also uses the approximation

$$\exp(\pi y)/\sinh\pi y\simeq 1/\pi y\,, \tag{18}$$

which is inacceptable for large y. The monopole rates are, therefore, substantially underestimated there.

The inclusion of higher multipoles and of penetration effects makes the Akylas-Vogel cascade program[4] lengthier and more cumbersome than the previous cascade.[3] Is it necessary?

There is no doubt that the individual rates are quite different in the two calculations. The differences usually increase with increasing quantum numbers. For transitions with the same n the differences are generally larger for more eccentric orbits. To illustrate how large the differences could be we compare in Fig. 4 the rates for the transitions originating in the $(n,l)=(17,2)$

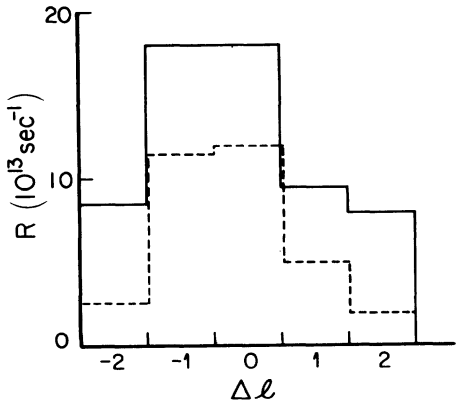

FIG. 4. Auger rates for the $n=17$, $l=2\to n'$, $l+\Delta l$ transitions in Al. The full histogram shows the sum over n' of rates calculated without penetrations; the dashed histogram shows the same quantity calculated including the penetration effect.

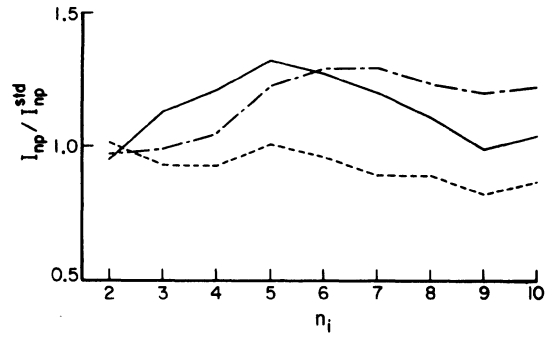

FIG. 5. Effect of various approximations on the Lyman series in Al. The displayed quantity is the x-ray intensity normalized to the standard value of Table III. [Notation: Full curve—normal treatment of monopoles, dipoles and quadrupoles calculated without penetration. Dashed curve—normal treatment of monopoles, dipoles without penetration, no quadrupoles. Dot-dashed curve—monopole rates reduced by the factor (18), dipoles without penetration, no quadrupoles.]

state of Al. The rates are plotted in histogram form as a function of the angular momentum change $\Delta l = l_{fi} - l_{in}$. The penetration effects reduce the total rate by a factor of 2 in this case. Curiously enough the total rate with penetration, that is the rate used in the present cascade calculation, and the total Hüfner cascade rate [dipoles without penetration + monopoles reduced by the factor (18)], differ by only 10%. This is so because the additional quadrupole and monopole rates in the new program to a large extent compensate the decreased dipole rate due to penetration. Similarly, when calculating the average angular momentum change $\langle \Delta l \rangle$ and the average $\langle \Delta n \rangle$ the two programs typically differ by ~20%.

Another way of illustrating the role of various terms is shown in Fig. 5. Starting with the identical l distribution and refilling rate we calculate the intensities of the Lyman series in Al. Exclusion of penetration or of individual multipoles leads to up to 30% change in intensity. Because the cascade analysis involves adjustable parameters, the two available programs would lead to differences of these parameters of a comparable magnitude. This should be compared to the experimental accuracy, which is better than 5% for the lower members of the various x-ray series. The simpler cascade code[3] is therefore useful for a preliminary analysis, but the more elaborate code[4] is needed when one wants to utilize the real accuracy of the directly experimentally determined quantities.

IV. CONCLUSIONS

The available experimental data on muonic x-ray intensities are analyzed in an unified way for the third-row elements, $Z = 11$–17. The only exception is Si where not enough data are presently available.

The analysis uses 3 adjustable parameters for each atom, plus an overall parameter describing the L-shell population. The parameters are found to vary smoothly with Z. The effective electron K width is fast increasing with Z. In Na it is 4 times smaller than the corresponding normal atom width; this reduction decreases to 1.5 in Cl.

The initial l distributions in all atoms studied are not very different from the statistical l distribution. Nevertheless, there is a pronounced tendency to have larger average angular momentum near closed atomic shells than in the middle of the shell. This effect was noted earlier[8-10] and is apparently present even to a larger degree in pionic and kaonic atoms.

The calculations show that the lengthier, but more accurate treatment using the Akylas-Vogel code is necessary when one wants to use the full accuracy of the experimental data. The treatment of electron refilling, including the L shell, emerges as the most uncertain part of the analysis. Other data, such as measurement of electron screening, could help to determine the relevant quantities. However, it is clear from the present analysis that in the light muonic atoms considered here the inner electron shells are heavily depleted during various stages of the muon cascade.

ACKNOWLEDGMENTS

Part of this work was done during the author's stay at the University of Fribourg. Discussions with Professor L. Schaller, Professor L. Schellenberg, and Professor H. Schneuwly, as well as the hospitality of Professor O. Huber are appreciated. This work was supported by the U. S. Department of Energy under Contract No. DE-AC-03-76-ER00063.

[1]G. R. Burbidge and A. H. de Borde, Phys. Rev. 89, 189 (1953).
[2]Y. Eisenberg and D. Kessler, Nuovo Cimento 19, 1195 (1961).
[3]J. Hüfner, program CASCADE.
[4]V. R. Akylas and P. Vogel, Comput. Phys. Commun. 15, 291 (1978).
[5]R. Bergmann, H. Daniel, P. Ehrhart, F. J. Hartmann,

H. J. Pfeiffer, J. J. Reidy, T. von Egidy, and W. Wilhelm, contribution to the VIIIth International Conference on High Energy Physics and Nuclear Structure, Vancouver, Canada, 1979 (unpublished).
[6]P. Vogel, P. K. Haff, V. Akylas, and A. Winther, Nucl. Phys. A 254, 445 (1975).
[7]M. Leon and J. H. Miller, Nucl. Phys. A282, 461 (1977).
[8]G. L. Godfrey and C. E. Wiegand, Phys. Lett. B 56, 255 (1975).
[9]R. M. Pearce, G. A. Beer, M. S. Dixit, S. K. Kim, J. A. Macdonald, G. R. Mason, A. Olin, C. Sabev, W. C. Sperry, and C. Wiegand, Can. J. Phys. 57, 2084 (1979).
[10]R. Bergmann, H. Daniel, T. von Egidy, F. J. Hartmann, J. J. Reidy, and W. Wilhelm, Z. Phys. A 291, 129 (1979).
[11]K. Kaeser, B. Robert-Tissot, L. A. Schaller, L. Schellenberg, and H. Schneuwly, Helv. Phys. Acta 52, 304 (1979).
[12]K. Kaeser, T. Dubler, B. Robert-Tissot, L. A. Schaller, L. Schellenberg, and H. Schneuwly, Helv. Phys. Acta 52, 238 (1979).
[13]L. Schellenberg (private communication).
[14]L. F. Mausner, R. A. Naumann, J. A. Monard, and S. N. Kaplan, Phys. Rev. A 15, 479 (1977).
[15]P. Vogel, Phys. Rev. A 8, 2292 (1973).
[16]W. Ruckstuhl, B. Aas, W. Beer, I. Beltrami, P. Ebersold, R. Eichler, M. Guanziroli, Th. V. Ledebur, H. J. Leisi, and W. W. Sapp, contribution to the VIIIth International Conference on High Energy Physics and Nuclear Structure, Vancouver, Canada, 1979 (unpublished).
[17]V. R. Akylas, Ph.D. thesis, California Institute of Technology, 1978 (unpublished).
[18]I. M. Band, M. B. Trzhaskovkaya, and M. A. Listengarten, At. Data Nucl. Data Tables 18, 433 (1976).
[19]M. Leon and R. Seki, Nucl. Phys. A298, 333 (1978).
[20]V. Bingeli, thesis, University of Basel, 1977 (unpublished).